Microchimica Acta (2020) 187: 6
https://doi.org/10.1007/s00604-019-3814-x

ORIGINAL PAPER

Carbon nanotube hollow polyhedrons derived from ZIF-8@ZIF-67 coupled to electro-deposited gold nanoparticles for voltammetric determination of acetaminophen

Yafeng Jin[1,2] · Xiaobo Li[2,3] · Chuangye Ge[2] · Jingjing Ma[2] · Yuanchao Li[2] · Erqing Zhao[2] · Shuwen Yao[2] · Guangri Xu[2] · Donghao Li[1]

Received: 21 April 2019 / Accepted: 12 September 2019 / Published online: 3 December 2019

Abstract

A comparative study was carried out on the electrochemical behavior of three carbonized zeolitic imidazolate frameworks (ZIFs) synthesized through solvothermal pyrolysis. An electrochemical sensor for acetaminophen (ACT) was subsequently developed. The sensor was made by coating the glassy carbon electrode (GCE) with cobalt-nitrogen co-doped carbon nanotube hollow polyhedron (Co-NCNHP), which was prepared from core shell ZIF-8@ZIF-67, before electrodeposition of gold nanoparticles. Due to the high specific surface area, good electrical conductivity and stability of both Co-NCNHP and the gold nanoparticles, the resultant sensor displayed excellent electrocatalytic activity towards ACT with the catalytic rate constant K_{cat} of 4.9×10^5 M^{-1} s^{-1}, diffusion coefficient D of 1.8×10^{-6} cm^2 s^{-1}, high sensitivity of 1.75 μA μM^{-1} cm^{-2}, and best at a working voltage of 0.35 V (vs. Ag/AgCl). Benefitting from the synergistic effect of both Co-NCNHP and gold nanoparticles, the modified GCE had a linear response in the 0.1 μM–250 μM ACT and detection limit of 0.05 μM (at $S/N = 3$). The sensor was successfully applied to quantify ACT in tablets and spiked urine samples with recoveries ranged between 96.0% and 105.2%.

Keywords Carbonized Zeolitic imidazolate framework · Solvothermal-pyrolysis · Cobalt- nitrogen co-doping · Acetaminophen · Electrochemical sensor

Introduction

Acetaminophen (ACT) is an antipyretic and analgesic medicine that reduces fever and relieve pain through inhibiting the synthesis of prostaglandins [1, 2]. However, long-term use or overdose of ACT may cause some severe harmful side effects including hepatocyte death, pancreas inflammation and kidney failure [3, 4]. As a result, it is highly necessary to set up a sensitive and stable method for ACT detection. Electrochemical analysis, especially for biological, clinical and environmental sample, has gained great popularity. Development of a sensitive and stable electrode modifier is of importance to overcome the low sensitivity of bare electrode. Various nanomaterials such as metal and metal oxide/metal hydroxide [5, 6], graphene [7], carbon nanotube [8], conductive polymer [9] and ionic liquid [10] have been used to modify bare electrodes for ACT detection. Houshmand et al. [5] studied electrocatalytic oxidation mechanisms of ACT on cobalt hydroxide nanoparticles modified GCE and successfully applied the sensor to analysis of ACT in human urine. Bui et al. [6] developed a sensor based on gold nanoparticles (AuNPs) and glutamic acid for detection of ACT in pharmaceutical. Higher electrocatalytic activity for ACT redox using graphitic-N-rich nitrogen-doped graphene was

Electronic supplementary material The online version of this article (https://doi.org/10.1007/s00604-019-3814-x) contains supplementary material, which is available to authorized users.

✉ Guangri Xu
xugr70@163.com

✉ Donghao Li
dhli6510@126.com

[1] Department of Chemistry, MOE Key Laboratory of Natural Resources of the Changbai Mountain and Functional Molecules, Yanbian University, Park Road 977, Yanji City 133002, Jilin Province, China

[2] School of Chemistry and Chemical Engineering, Henan Institute of Science and Technology, Xinxiang 453003, China

[3] State Key Laboratory of Luminescent Materials and Devices, South China University of Technology, Guangzhou 510641, China

obtained than that of graphitic-N-free nitrogen-doped graphene by Cao et al. [7]. Alothman et al. [8] achieved simultaneous determination of ACT and dopamine using multi-walled carbon nanotubes modified GCE. It is conceivable that a modifier rich of Co, Au, N and CNTs is promising for ACT monitoring.

Metal-organic frameworks (MOFs), which are composed of inorganic metal irons/clusters and organic ligands, have drawn increasing attention in field of electrochemistry because of their large specific area, tunable internal pore size and functionalization [11, 12]. Zeolitic imidazolate frameworks (ZIFs), as a typical subgroup of MOFs, are rich of carbon, nitrogen and transition metals (e.g., Zn^{2+}, Co^{2+}). ZIFs can be synthesized cheaply and transformed conveniently into nitrogen-doped nanoporous carbon (NPC) for improving their conductivity and mechanical strength [13]. In addition, NPC derived from ZIFs has further proved of outstanding electrocatalytic activity in electrochemical fields. Gai et al. [14] synthesized NPC derived from ZIF-8 to modify the electrode for detection of ascorbic acid, dopamine and uric acid simultaneously. Yue et al. [15] fabricated Prussian blue/NPC/polypyrrole/GCE sensor for monitoring hydrazine based on carbonized ZIF-67. Although the single C-ZIF-8 or C-ZIF-67 has been applied in electrochemical analysis, electrochemical performance of the carbonized hybrid ZIFs like carbonized core-shell ZIF-8@ZIF-67 as well as the difference among them, has rarely been explored.

Inspired by the above, three kinds of carbonized ZIFs, namely C-ZIF-8, C-ZIF-67 and Co-NCNHP, were synthesized and comparatively studied. The best among the three, Co-NCNHP was then coupled with AuNPs via potentiostatic deposition to construct the sensor for electrochemically sensing ACT. The electrochemical parameters including the deposition time of AuNPs, pH value, scan rate, diffusion coefficient and catalytic rate constant for ACT on modifying sensor were optimized. The modified sensor was used to determine ACT in tablets and urine samples.

Experimental section

Reagents

Zinc nitrate hexahydrate ($Zn(NO_3)_2{\cdot}6H_2O$), cobalt nitrate hexahydrate ($Co(NO_3)_2{\cdot}6H_2O$), 2-methylimidazole (2-MeIm), $HAuCl_4{\cdot}3H_2O$, acetaminophen (ACT) and chitosan were purchased from Aladdin Biochemical Technology Co. Ltd. (Shanghai, China, www.aladdin-reagent.com). The ACT was in 0.1 M phosphate buffer (PB, pH 7), which was made up of sodium phosphate dibasic and sodium dihydrogen phosphate. All the regents were used directly without further dispose and the aqueous solution was freshly prepared with deionized water.

Characterization

Scanning electron microscope (SEM) of Hitachi SU8010 (Hitachi, Japan https://www.hitachi.com/) and transmission electron microscope (TEM) of Hitachi HT7700 (Hitachi, Japan https://www.hitachi.com/) were used to explore the morphology and structure nature. X-ray diffraction (XRD) was measured on Bruker AXS D8 Advance diffractometer (Bruker, Germany, https://www.bruker.com/), N_2-adsorption-desorption analysis was tested on MicroActive for ASAP 2460 (Micromeritics, USA, https://www.micromeritics.com/), X-ray photoelectron spectroscopy (XPS) was performed on Thermo Scientific ESCALAB 250Xi (ThermoFisher Scientific, USA, https://www.thermofisher.com/).

Electrochemical measurements

All the electrochemical measurements, including cyclic voltammetry (CV), electrochemical impedance spectroscopy (EIS), differential pulse voltammetry (DPV), and amperometric i-t curve method were performed via CHI 900 electrochemical workstation (Shanghai CH Instrument, China, http://www.chinstr.com/) at ambient temperature. A three-electrode system was used, which contained working electrode of glassy carbon electrode (GCE, diameter: 3.0 mm), counter electrode of platinum wire electrode, and the reference electrode of Ag/AgCl electrode. The electrochemical characterization of the different modified electrodes were analyzed by CV and EIS in 5 mM $[Fe(CN)_6]^{3-/4-}$ (1:1) solution containing 0.1 M KCl. CV was taken between −0.1 and 0.6 V at a scan rate of 100 mV s^{-1}, and EIS was obtained under an open circuit potential about 0.2 V, amplitude of 0.005 V and frequency range of 0.1 to 10^5 Hz. The electrochemical behavior of different modified electrodes for ACT sample (0.1 M PB, pH 7) were investigated by CV and DPV. CV was recorded between −0.1 and 0.8 V at a scan rate of 100 mV s^{-1}. The DPV was analyzed from 0.1 to 0.6 V. Amperometric i-t curve was performed at 0.35 V with solution stirring rate of 1500 rpm.

Synthesis of Co-NCNHP

The method for synthesis of Co-NCNHP and other materials (ZIF-8, ZIF-67, ZIF-8@ZIF-67, C-ZIF-8 and C-ZIF-67) is largely on the basis of reference [16]. The detailed procedure is shown in Electronic Supporting Material.

Fabrication of Au/Co-NCNHP/GCE sensor

The bare GCE was polished with aluminum oxide powder (0.05 μm) slurry to mirror-like clearness. Then it was rinsed with water and dried at ambient temperature. After that, 1 mg Co-NCNHP was added into 1 mL chitosan aqueous solution (1‰ acetic acid, volume ratio) to get a suspension, 5 μL of

which was dropped on the GCE surface before dried under infrared lamp. Afterwards, AuNPs were electrodeposited on the bottom of GCE via reduction of 5 mM $HAuCl_4 \cdot 3H_2O$ aqueous solution for 15 s at 0.4 V. The modified electrode was denoted as Au/Co-NCNHP/GCE. All the other sensors including C-ZIF-8/GCE, C-ZIF-67/GCE, Co-NCNHP/GCE, ZIF-8@ZIF-67/GCE and Au/GCE were fabricated by the same way. The procedure for fabrication of the sensor is shown in Scheme 1.

Preparation of real sample

The ACT tablet (labelled 300 mg per tablet, http://www.wtyy.com.cn/cn/) was obtained from local pharmacy. Firstly, each tablet was ground completely and dissolved with water under stirring. Then the sample solution was filtered by syringe filter membrane with the pore diameter of 0.45 μm. Lastly, the tablet sample solution was diluted with PB (pH 7) to different concentration (10 μM, 100 μM and 200 μM) of ACT sample. In the case of human urine sample, it was supplied from healthy volunteer (the first author of this paper) and diluted ten times with PB (pH 7) directly. Then the standard spiked method was used for calculation of ACT recoveries before DPV test.

Results and discussion

Choice of materials

Carbonized ZIFs, a kind of NPC, are widely applied in electrocatalytic field for their fascinating chemical and mechanical stability, as well as good electrical conductivity. Many merits cannot be retained through the synthesis by pyrolysis of a single ZIF. Pyrolysis of a core-shell ZIF-8@ZIF-67 was carried out for better electrocatalyst. This nanomaterial not only exhibits high specific surface area, large pore volume, but reveals highly graphitic structure. Besides, the Co, N and CNT are all existent at the same structure. When coupled to AuNPs, the composite material displays excellent electrochemical activity for ACT redox. Compared with other conducting polymers, or carbon nanomaterial or metallic oxide such as PPy, PANI, rGO, C-dots, ZnO and etc. Au/Co-NCNHP is endowed with the advantages of high sensitivity and robust stability. The difference between C-ZIF-8, C-ZIF-67 and Co-NCNHP was studied as well.

Physical characterization

The XRD patterns of C-ZIF-8, C-ZIF-67, Co-NCNHP and Au/Co-NCNHP are shown in Fig. 1a. For C-ZIF-8, there are two obvious peaks at 25° and 44°, which are assigned to the amorphous carbon. For C-ZIF-67 and Co-NCNHP, the (002) peak is shifted towards 26°, suggesting the presence of graphitic carbon. Peaks at 44.3°, 51.5° and 76.1°correspond to (111), (200) and (220) characteristic diffraction peaks of Co (JCPDS 15–0806) respectively. It manifests that we have synthesized the Co-NCNHP faultlessly. As shown in the pattern of Au/Co-NCNHP, the peaks of Au are located at 38.42° (111), 44.14° (200), 64.39° (220) and 77.48° (311). By contrast, the peaks of Co are somewhat weaker, which might be due to the chitosan and AuNPs covered on the Co-NCNHP partially. The result confirms that the AuNPs have been deposited onto Co-NCNHP evenly. The XRD characterization of synthesized ZIF-8, ZIF-67 and ZIF-8@ZIF-67 further proves the validation of our synthesis strategy, see Fig. S1 in Electronic Supporting Material (ESM).

TEM and EDS mapping images in Fig. 1b and c reveal that C, N distribute evenly in ZIF-8@ZIF-67, whereas Zn is mainly located at the center, and Co is located around the Zn cluster, suggesting we have fabricated the core-shell ZIF-8@ZIF-67 structure. Figure 1d, e and Fig. S2 show that the synthesized Co-NCNHP is a hollow polyhedron (about 400 nm) with lots of CNTs. Note that, neither the single C-ZIF-8 nor C-ZIF-67 has CNTs (Fig. S3), which is in accordance with the

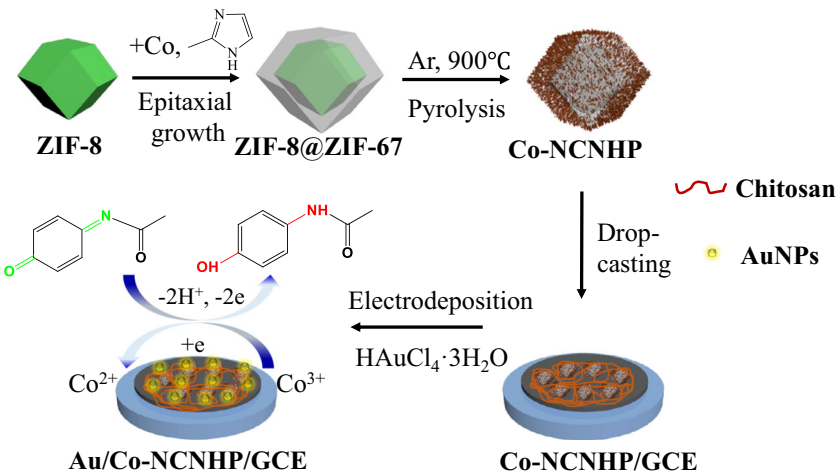

Scheme 1 The fabrication procedure and the reaction mechanism of the Au/Co-NCNHP/GCE for ACT detection

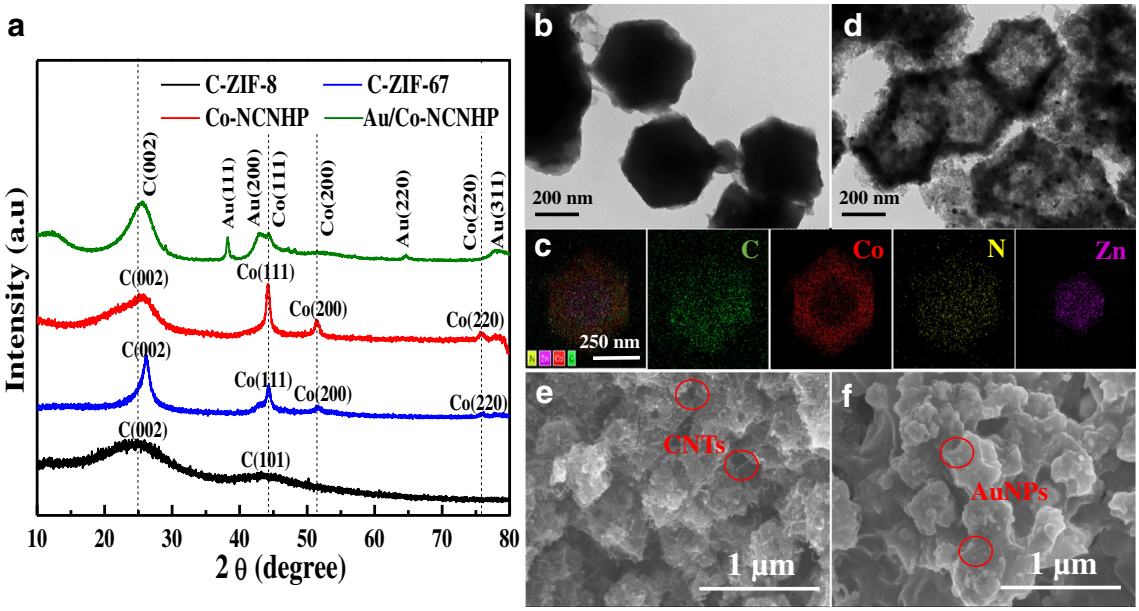

Fig. 1 (**a**) XRD patterns of synthesized C-ZIF-8 (black line), C-ZIF-67 (blue line), Co-NCNHP (red line) and Au/Co-NCNHP (green line). TEM images of (**b**) ZIF-8@ZIF-67 and (**d**) Co-NCNHP. (**c**) EDS mapping images of ZIF-8@ZIF-67. SEM images of (**e**) Co-NCNHP and (**f**) Au/Co-NCNHP

reference [16]. Therefore, it can be concluded that we synthesized the Co-NCNHP with success. As shown in Fig. 1f and S4, AuNPs are located uniformly on the film of Co-NCNHP with the help of chitosan.

Three types of N can be noticed in N 1 s spectrum of Fig. 2a. These are assigned to pyridinic N (398.6 eV, 32.1%), graphitic N (401.3 eV, 39.2%) and oxidized-N (403.8 eV, 28.6%). It is clear that there is no pyrrolic N, because stability of the pyridinic N and graphic N is stronger than that of pyrrolic N [17]. The percentage of pyridinic N and graphic N is so high that it can improve the electrocatalytic activity and stability of Co-NCNHP [18]. Co 2p spectrum in Fig. 2b indicates that there are two peaks at 778.8 eV and 780.2 eV, corresponding to metallic Co and N-coordinated Co^{2+} ($Co\text{-}N_x$) respectively.

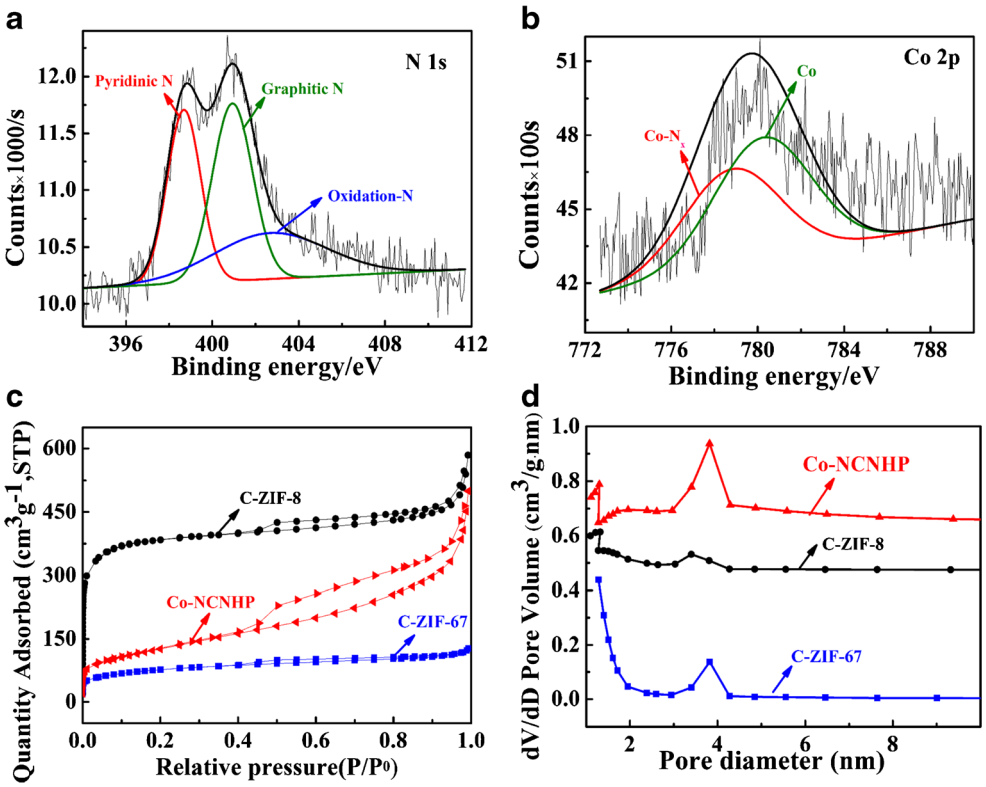

Fig. 2 (**a**) N 1 s spectrum and (**b**) Co 2p spectrum of Co-NCNHP. (**c**) N_2 adsorption-desorption isotherm (**d**) pore diameter distribution of the C-ZIF-8, C-ZIF-67 and Co-NCNHP

The existence of Co and Co^{2+} is also helpful for ACT redox [5]. Other element characterization is shown in Fig. S5.

The specific surface area and pore distribution information are shown in Fig. 2c. The N_2 adsorption-desorption curves of the three carbonized ZIFs present the IV type isotherms, with sharp appearance due to the microspores when the relative pressure (RP) under 0.05. Then the curves increase slowly when the RP is between 0.05 and 0.45. With the RP over 0.45, the hysteresis loops of desorption curves are observed, indicating the presence of abundant mesopores. This is also supported by pore diameter distribution in Fig. 2d, pore diameters of the three carbonized ZIFs being 3–5 nm. This pore distribution is beneficial for mass transport in aqueous electrolyte [18]. Table S1 presents the surface area and pore volume of the foregoing three carbonized ZIFs. Obviously, C-ZIF-8 possesses the largest BET surface area (1480 $m^2\ g^{-1}$), while that of C-ZIF-67 is the smallest (278 $m^2\ g^{-1}$). This may be due to the collapse of micropores for C-ZIF-67 caused by graphitization of amorphous carbon [19]. As expected, Co-NCNHP has a middle value of 461 $m^2\ g^{-1}$, and the pore volume is the largest (0.77 $cm^3 \cdot g^{-1}$).

Electrochemical characterization of C-ZIF-8, Co-NCNHP and C-ZIF-67

To compare the electrochemical behavior of the carbonized ZIFs, we tested the three electrodes in potassium ferricyanide solution via CV scanning for successive 100 circles. The surface areas A of different electrodes were also calculated in the solution above. The detailed process and results are shown in the section of Results and discussion in ESM. Figure 3a shows that the highest anodic peak current density I_{pcd} of 0.69 mA cm^{-2} is achieved on C-ZIF-8/GCE, and the I_{pcd} of Co-NCNHP/GCE (0.67 mA cm^{-2}) ranks the second. However, the peak separation $\triangle E_p$ of 207 mV on the C-ZIF-8/GCE is not as good as that of Co-NCNHP/GCE ($\triangle E_p$ = 130 mV). It suggests that the Co-NCNHP owns the second highest sensitivity and the best reversibility among them. The reasons may be illustrated as follows: for one thing, larger specific surface area results in more exposed active sites. Therefore, the catalytic efficiency for the target molecule will be improved [20, 21]. Large specific surface area value of the Co-NCNHP contributed to its good electrochemical activity. For another, the electrical conductivity mainly depends on the graphitic degree or some heteroatom in carbon nanomaterial [16, 22]. SEM, TEM, EDS mapping and XPS prove there are not only Co and N, but also lots of CNTs on Co-NCNHP, which contrasts to the C-ZIF-8 or C-ZIF-67. The reasons above illustrate the excellent electrochemical performance of Co-NCNHP. In order to examine the stability of the materials, we extracted the anodic peak current values from 1st, 20th, 40th, 60th, 80th, 100th circle of each electrode, and calculated the relative standard deviation (RSD) of C-ZIF-8/GCE, Co-NCNHP/GCE and C-ZIF-67/GCE, being 9.8%, 1.4% and 0.22%, respectively. C-ZIF-67 exhibits the strongest stability among them. This is probably because the graphitic carbon has a better stability than amorphous carbon. In consideration of the sensitivity and stability, the Co-NCNHP is the best electrocatalyst in this case.

To evaluate the electron conductivity of the three kinds of carbonized ZIFs, we further measured the electrochemical impedance of them. As shown in Fig. 3b, the smallest impedance value was obtained on Co-NCNHP (83 Ω), implying it possesses the best electron transfer ability among them. On the contrary, the C-ZIF-8 exhibits a weaker electron conductivity of 110 Ω.

The electrochemical behavior of different electrodes for ACT

The electrochemical behavior of the three carbonized ZIFs towards ACT was compared via CV. It is shown in Fig. 4a that the largest redox peaks densities and good reaction reversibility are obtained on Co-NCNHP/GCE. Fig. S6 shows there is a pair of redox peaks at 0.2 V for Co-NCNHP/GCE in PB, which is attributed to the redox of Co^{2+}/Co^{3+} [23], revealing this reaction probably facilitates ACT redox. Therefore, Co-NCNHP was chosen for our further experiment.

In order to improve the sensibility and stability of the sensor, we coupled AuNPs to Co-NCNHP by electrodeposition.

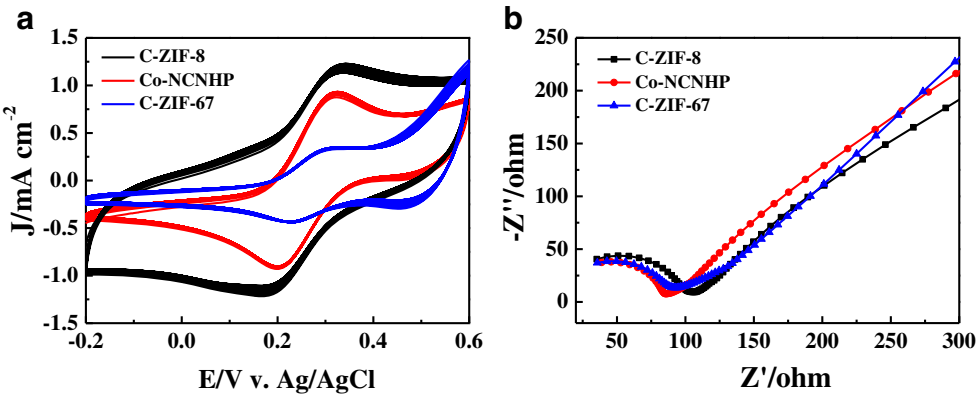

Fig. 3 (**a**) CV scans of successive 100 circles and (**b**) EIS of C-ZIF-8/GCE, Co-NCNHP/GCE and C-ZIF-67/GCE in 5 mM $[Fe(CN)_6]^{3-/4-}$ (1:1) solution with 0.1 M KCl. Scan rate: 100 mV s^{-1}

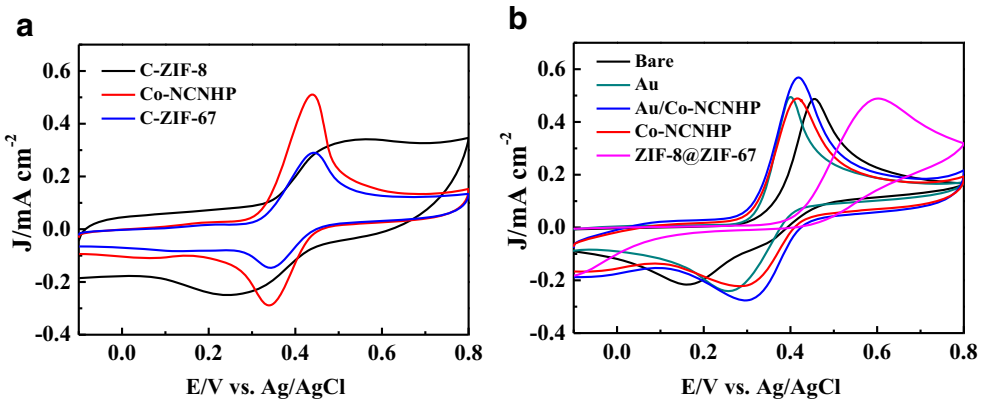

Fig. 4 (**a**) CV scans of C-ZIF-8/GCE, Co-NCNHP/GC and C-ZIF-67/GCE in 0.1 M PB (pH 7) containing 1 mM ACT. (**b**) CV scans of bare GCE, Au/GCE, ZIF-8@ZIF-67/GCE, Co-NCNHP/GCE and Au/Co-NCNHP/GCE in 0.1 M PB (pH 7) containing 1 mM ACT. Scan rate: 100 mV s^{-1}

The electrochemical behavior of the five electrodes were studied by CV in 1 mM ACT. As shown in Fig. 4b, Au/Co-NCNHP/GCE exhibits the largest redox peaks current densities compared with others. Only oxidation peak is observed on ZIF-8@ZIF-67/GCE. Redox currents densities of both Au/GCE and Co-NCNHP/GCE are larger than that of bare GCE. The anodic peak potential (E_{pa}) and cathodic peak potential (E_{pc}) of bare GCE are at 455 mV and 159 mV respectively, with a peak separation ($^{\triangle}E_p$) of 296 mV. Meanwhile, the $^{\triangle}E_p$ values of Au/GCE, Co-NCNHP/GCE and Au/Co-NCNHP/GCE are 146 mV, 125 mV and 122 mV respectively. Therefore, the Au/Co-NCNHP presents good electron transport ability and catalytic rate toward the oxidation of ACT, and the electrochemical performance of Co-NCNHP is better than non-carbonized ZIF-8@ZIF-67.

The possible reaction mechanism for ACT on the Au/Co-NCNHP sensor is discussed as follows: (i) For Co-NCNHP, the large specific surface and pore volume lead to more active sites exposed, implying more targets can be adsorbed in a short time. The Co-NCNHP is rich of π electrons, which can strongly adsorb molecules with aromatic rings. In case of the Co, N and CNTs, not only are they helpful to improve the electron conductivity, but the redox of Co^{2+}/Co^{3+} is likely to promote the ACT redox. (ii) The AuNPs are famous for their superior conductivity, large specific area, and stability. Hence, the AuNPs facilitate the electrocatalysis activity and conductivity of the interface. (iii) The synergistic effect between Co-NCNHP and AuNPs contributes to the excellent electrochemical redox of ACT. The probable reaction is described as Scheme 1.

Optimization of conditions

The following parameters were optimized: (a) sample pH value; (b) deposition time. Respective data and figures are given in Fig. S7a and b. The following experimental conditions were found to give best results: (a) best sample pH value: 7; (b) deposition time: 15 s.

Effect of scan rate

Effect of scan rate toward ACT redox on the sensor was also investigated. Fig. S7c displays that the redox peak current is proportional to the square root of scan rate. The liner equation between I_{pa}, I_{pc} and scan rate is expressed as I_{pa} (μA) = 7.0593 v [(mV·s^{-1})$^{1/2}$] - 13.7680, I_{pc} (μA) - 3.7750 v [(mV·s^{-1})$^{1/2}$] + 7.2457. It reveals the process of ACT redox on the Au/Co-NCNHP/GCE is controlled by diffusion.

Chronoamperometry determination of ACT

The ACT oxidation at the sensor was also studied by chronoamperometry (Fig. S7d). The catalytic rate constant and diffusion coefficient are two important parameters for electrochemical reaction. The catalytic rate constant can be calculated by the equation:

$$\frac{I_{cat}}{I_l} = (\pi k_{cat} ct)^{1/2} \quad (1)$$

Where I_{cat} stands for the catalytic current produced on the Au/Co-NCNHP/GCE for ACT. I_L means the limited current in absence of ACT. c and t are the bulk concentration of ACT solution and the time, respectively. From the left insert of Fig. S7d, we can obtain the K_{cat} of 4.94×10^5 M^{-1} s^{-1}. Besides, from the equation:

$$I = \mathrm{nFA}D^{1/2}c\pi^{-1/2}t^{-1/2} \quad (2)$$

Where I (A) refers to the peak current, n is the number of electron taking part in the redox, A (cm^{-1} s^{-1}) is the efficient area of electrode, D(cm^2 s^{-1}) is the diffusion coefficient, and c (mol L^{-1}) is the concentration of ACT. We can also evaluate the diffusion coefficient D of 1.81×10^{-6} cm^2 s^{-1}.

Quantitative determination of ACT

The feasibility of the Au/Co-NCNHP/GCE in ACT determination was validated by DPV. As presented in Fig. 5a, the

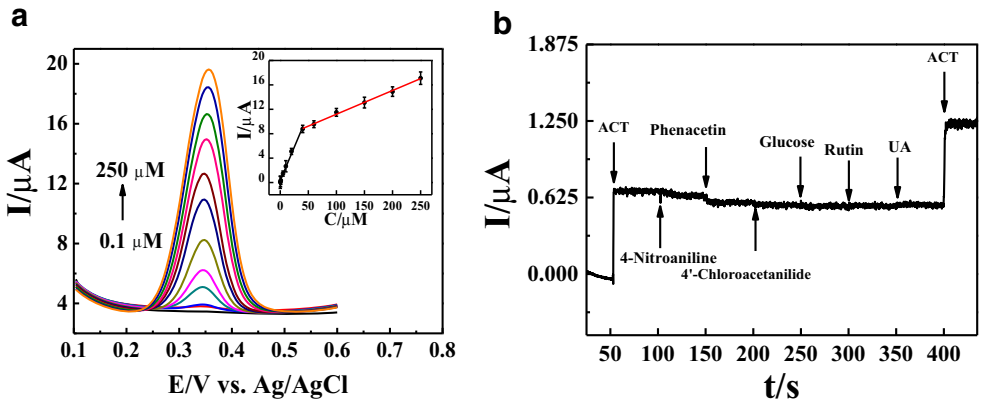

Fig. 5 (**a**) DPV response of Au/Co-NCNHP/GCE in 0.1 M PB containing different concentration of ACT (0.1, 0.5, 1, 5, 10, 20, 40, 60, 100, 150, 200, 250 μM, pH 7). Insert plot is the calibration plot of ACT. (**b**) Amperometric response towards 1 mM ACT in presence of 4-Nitrioaniline (5 mM), Phecantin (5 mM), 4'-Chloroacetanilide (5 mM), Glucose (10 mM), Rutin (1 mM), uric acid (UA, 1 mM) in 0.1 M PB (pH 7.0). Voltage: 0.35 V. Stirring rate: 1500 rpm

anodic peak current is in proportion to the concentration of ACT with two linear segments. The linear equations are as follows: I_{pa} (μA) = 0.2189C (μM) + 0.3275 (0.1–40 μM, R^2 = 0.9909), I_{pa} (μA) = 0.0389C (μM) + 7.3028, (40–250 μM, R^2 = 0.9952). The LOD is 0.05 μM, and the sensitivity of 1.75 μA μM^{-1} cm^{-2}. The method is compared with others as listed in Table 1 [24–33]. It is noticed that the linear range and LOD of the Au/Co-NCNHP/GCE are comparable to many other methods. The result suggests that both the Co-NCNHP and the AuNPs improve the electrochemical activity of the sensor for ACT determination.

Selectivity, reproducibility and stability

Selectivity is an important feature of the sensor to detect target with many interferences. In order to examine the selectivity, chemical structure-related drugs like 4-Nitroaniline (5 mM), Phenacetin (5 mM), 4'-Chloroacetanilide (5 mM), and some common biological substances with the close redox potential such as glucose (10 mM), rutin (1 mM), uric acid (UA, 1 mM) were used as the interference towards 1 mM ACT in 7 mL PB with the stirring speed of 1500 rpm. The volume of each substance was 100 μL and the time interval of adding the

Table 1 Comparison of different electrodes for determination of ACT

Electrode	Method	Linear range (μM)	LOD (μM)	Reference
PANI-MWCNT/GCE	DPV	1–100, 250–2000	0.250	[24]
Pt-Co/NPs/3,4,DHPID/CPE	SWV	1.0–850	0 .600	[25]
Fc-SAu/CNC/graphene/GCE	DPV	0.5–46, 46–275	0.100	[26]
$(MWCNT-G4.0)_6$/GCE	DPV	0.3–200	0.100	[27]
Graphene nanosheets/GCE	DPV	0.004–7.6	0.0007	[28]
MWCNT-PDDA-FPS	DPV	3–1100	0.600	[29]
PdNP@Al_2O_3/CPE	DPV	0.04–1400	0.036	[30]
P-RGO/GCE	DPV	1.5–120	0.360	[31]
Carbon@Co nanocages/Nafion /Poly tiopronin/GCE	DPV	0.5–225	0.170	[32]
Au/UiO-66-NH_2/GCE	DPV	0.12–95.10	0.049	[33]
Au/Co-NCNHP/GCE	DPV	0.1–40, 40–250	0.050	This work

Pt-Co/NPs/3, 4, DHPID/CPE: Pt-Co nanoparticles and 2-(3, 4-dihydroxyphenethyl) isoindoline-1, 3-dione/ carbon paste electrode; Fc-SAu/CNC/graphene/GCE: Thiol functional ferrocene derivative (Fc-SH) stabilized AuNP/ carbon dots nanocomposite /graphene; (MWCNT-G4.0)6/GCE: Multiwalled carbon nanotube (MWCNT) and the fourth generation poly(amidoamine) dendrimers (G4.0 PAMAM); MWCNT-PDDA-FPS: Multi-walled carbon nanotubes-ploy-diallyl-dimethyl-ammonium chloride-FPS; P-RGO: Phosphorus-doped graphene

Table 2 Determination of ACT in tablets and human urine

Sample	Prepared (μM)	Detected (μM)	RSD% ($n = 3$)	Recovery%
Tablets	10.0	9.7	2.5	97.0
	100.0	99.0	0.5	99.0
	200.0	210.4	2.8	105.2
Urine	10.0	9.6	1.2	96.0
	100.0	102.6	3.6	102.6
	200.0	195.0	4.0	97.5

samples was 50 s. Figure 5b demonstrates the interference have no significant impact on the target of ACT. The relative error is less than ±5.0%, indicating a good selectivity of the sensor. As for the reproducibility, as shown in Fig. S8, Table S2, the RSD for ACT determination is 1.6% at the same electrode ($n = 5$). As for different electrodes (n = 5), the mean RSD is 4.5%. To study the long-term stability, the modified sensor Au/Co-NCNHP/GCE was stored in refrigerator at 4 °C for ten days, then used to detect ACT. As shown in Fig. S9, the peak current retained about 90.0% of the initial peak current (RSD = 3.0, $n = 3$). So the long-term stability of the sensor is not so good. The reason may be due to the effect of chitosan binder or the storage condition. The long-term stability of the sensor can be improved by using other binder or eletrodeposition method or changing the storage condition.

Real sample analysis

To estimate the practical application of Au/Co-NCNHP/GCE, tablet sample and urine sample were analyzed with the sensor by DPV. Table 2 reveals that the recoveries of tablet sample are between 97.0%–105.2%, and the recoveries of urine sample are from 96.0% to 102.6%, indicating a great potential for determination of ACT in real samples.

Conclusions

We compared the electrochemical property of three carbonized ZIFs, and fabricated a novel Au/Co-NCNHP/GCE electrode for ACT determination. Due to the synergistic effects of Co-NCNHP and AuNPs, the sensor exhibits a good selectivity and reproducibility. For ACT determination in ACT tablets and spiked urine samples, satisfactory recoveries were received. The work provides a reference for the carbonized ZIFs to detect other substances of biologic interest, as well as an approach to detect the ACT in real sample. For the limitation of the method, more efforts should be made to investigate the aging process of the sensor and improve the long-term stability in future.

Acknowledgments This work was supported by the Open Fund of the State Key Laboratory of Luminescent Materials and Devices in South China University of Technology (NO. 2018-skllmd-09), the Key Research Projects for Institutions of Higher Education from the Department of Education, Henan Province (NO. 17A150010) and the National Natural Science Foundation of China (NO. 21703057). We also sincerely thank Dr. Haibo Shang, Dr. Wanqing Zhang, Miao Zhang, as well as Experimental Management Center of Henan Institute of Science and Technology for their help during the preparation of this paper.

Compliance with ethical standards The author(s) declare that they have no competing interests.

References

1. Dinis TCP, Madeira VMC, Almeida LM (1994) Action of phenolic derivatives (acetaminophen, salicylate, and 5-aminosalicylate) as inhibitors of membrane lipid peroxidation and as peroxyl radical scavengers. Arch Biochem Biophys 315:161–169
2. Fleckenstein AE, Volz TJ, Riddle EL, Gibb JW, Hanson GR (2007) New insights into the mechanism of action of amphetamines. Annu Rev Pharmacol Toxicol 47:681–698
3. Newton JF, Kuo CH, DeShone GM, Hoefle D, Bernstein J, Hook JB (1985) The role of p-aminophenol in acetaminophen-induced nephrotoxicity: effect of bis(p-nitrophenyl) phosphate on acetaminophen and p-aminophenol nephrotoxicity and metabolism in Fischer 344 rats. Toxicol Appl Pharmacol 81:416–430
4. Moss JL, Brown BW, Pai S-L, Torp KD, Aniskevich S (2018) Fulminant hepatic failure after simultaneous kidney-pancreas transplantation: a case report. Braz J Anesthesiol 68:535–538
5. Houshmand M, Jabbari A, Heli H, Hajjizadeh M, Moosavi-Movahedi AA (2008) Electrocatalytic oxidation of aspirin and acetaminophen on a cobalt hydroxide nanoparticles modified glassy carbon electrode. J Solid State Electrochem 12:1117–1128
6. Bui MPN, Li CA, Han KN, Pham XH, Seong GH (2012) Determination of acetaminophen by electrochemical co-deposition of glutamic acid and AuNP. Sensors Actuators B Chem 174:318–324
7. Cao Y, Si W, Zhang Y, Hao Q, Lei W, Xia X, Li J, Wang F (2018) Nitrogen-doped graphene: effect of graphitic-N on the electrochemical sensing properties towards acetaminophen. Flat Chem 9:1–7
8. Alothman ZA, Bukhari N, Wabaidur SM, Haider S (2010) Simultaneous electrochemical determination of dopamine and acetaminophen using multiwall carbon nanotubes modified glassy carbon electrode. Sensors Actuators B Chem 146:314–320
9. Boopathi M, Won M-S, Shim YB (2004) A sensor for acetaminophen in a blood medium using a cu(II)-conducting polymer complex modified electrode. Anal Chim Acta 512:191–197
10. Pourtaheri E, Taher MA, Beitollahi H (2018) Synergistic signal amplification based on ionic liquid-$BaTiO_3$ nanoparticle carbon paste electrode for sensitive voltammetric determination of acetaminophen. Anal Bioanal Chem Res 5:261–271
11. Dey C, Kundu T, Biswal BP, Mallick A, Banerjee R (2014) Crystalline metal-organic frameworks (MOFs): synthesis, structure and function. Acta Crystallogr Sect B: Struct Sci Cryst Eng Mater 70:3–10
12. Kempahanumakkagari S, Vellingiri K, Deep A, Kwon EE, Bolan N, Kim KH (2018) Metal-organic framework composites as electrocatalysts for electrochemical sensing applications. Coord Chem Rev 357:105–129
13. Zhang Y, Zhu R, Cui Y, Zhong J, Zhang X, Chen J (2014) Pt Ru nanoparticles supported on nitrogen-doped polyhedral mesoporous

carbons as electrocatalyst for methanol oxidation. Nanotechnology 25:135607
14. Gai P, Zhang H, Zhang Y, Liu W, Zhu G, Zhang X, Chen J (2013) Simultaneous electrochemical detection of ascorbic acid, dopamine and uric acid based on nitrogen doped porous carbon nanopolyhedra. J Mater Chem B 1:2742–2749
15. Zhao J, Yue P, Tricard S, Pang T, Yang Y, Fang J (2017) Prussian blue (PB)/carbon nanopolyhedra/polypyrrole composite as electrode: a high performance sensor to detect hydrazine with long linear range. Sensors Actuators B Chem 251:706–712
16. Pan Y, Sun K, Liu S, Cao X, Wu K, Cheong WC, Chen Z, Wang Y, Li Y, Liu Y, Wang D, Peng Q, Chen C, Li Y (2018) Core-shell ZIF-8@ZIF-67-derived CoP nanoparticle-embedded N-doped carbon nanotube hollow polyhedron for efficient overall water splitting. J Am Chem Soc 140:2610–2618
17. Deng D, Pan X, Yu L, Cui Y, Jiang Y, Qi J, Li WX, Fu Q, Ma X, Xue Q, Sun G, Bao X (2011) Toward N-doped graphene via solvothermal. Chem Mater 23:1188–1193
18. Lai L, Potts JR, Zhan D, Wang L, Poh CK, Tang C, Gong H, Shen Z, Lin J, Ruoff RS (2012) Exploration of the active center structure of nitrogen-doped graphene-based catalysts for oxygen reduction reaction. Energy Environ Sci 5:7936–7942
19. Liang C, Li Z, Dai S (2008) Mesoporous carbon materials: synthesis and modification. Angew Chem Int Ed 47:3696–3717
20. Shao Y, Wang J, Wu H, Liu J, Aksay IA, Lin Y (2010) Graphene based electrochemical sensors and biosensors: a review. Electroanalysis 22:1027–1036
21. Wang T, Kou Z, Mu S, Liu J, He D, Amiinu IS, Meng W, Zhou K, Luo Z, Chaemchuen S, Verpoort F (2018) 2D dual-metal zeolitic-imidazolate-framework-(ZIF)-derived bifunctional air electrodes with ultrahigh electrochemical properties for rechargeable zinc-air batteries. Adv Funct Mater 28:1705048
22. Tang J, Salunkhe RR, Liu J, Torad NL, Imura M, Furukawa S, Yamauchi Y (2015) Thermal conversion of core-shell metal-organic frameworks: a new method for selectively functionalized nanoporous hybrid carbon. J Am Chem Soc 137:1572–1580
23. Shi L, Li Y, Cai X, Zhao H, Lan M (2017) ZIF-67 derived cobalt-based nanomaterials for electrocatalysis and nonenzymatic detection of glucose: difference between the calcination atmosphere of nitrogen and air. J Electroanal Chem 799:512–518
24. Li M, Jing L (2007) Electrochemical behavior of acetaminophen and its detection on the PANI-MWCNTs composite modified electrode. Electrochim Acta 52:3250–3257
25. Karimi-Maleh H, Hatami M, Moradi R, Khalilzadeh MA, Amiri S, Sadeghifar H (2016) Synergic effect of Pt-co nanoparticles and a dopamine derivative in a nanostructured electrochemical sensor for simultaneous determination of N-acetylcysteine, paracetamol and folic acid. Microchim Acta 183(11):2957–2964
26. Yang L, Huang N, Lu Q, Liu M, Li H, Zhang Y, Yao S (2016) A quadruplet electrochemical platform for ultrasensitive and simultaneous detection of ascorbic acid, dopamine, uric acid and acetaminophen based on a ferrocene derivative functional AuNP/carbon dots nanocomposite and graphene. Anal Chim Acta 903:69–80
27. Zhang Y, Liu X, Li L, Guo Z, Xue Z, Lu X (2016) An electrochemical paracetamol sensor based on layer-by-layer covalent attachment of MWCNTs and a G4.0 PAMAM modified GCE. Anal Methods 8:2218–2225
28. Song X, Fu J, Wang J, Li C, Liu Z (2018) Simultaneous voltammetric determination of acetaminophen and dopamine using a glassy carbon electrode modified with copper porphyrin-exfoliated graphene. Microchim Acta 185(8):369
29. Chen Y, Liu X, Wu T, Hou W, Liu M, Zhang Y, Yao S (2018) Enhanced electrochemical sensitivity towards acetaminophen determination using electroactive self-assembled ferrocene derivative polymer nanospheres with multi-walled carbon nanotubes. Electrochim Acta 272:212–220
30. Soltani N, Tavakkoli N, Shahdost-fard F, Salavati H, Abdoli F (2019) A carbon paste electrode modified with Al_2O_3-supported palladium nanoparticles for simultaneous voltammetric determination of melatonin, dopamine, and acetaminophen. Microchim Acta 186:540
31. Zhang X, Wang KP, Zhang LN, Zhang YC, Shen L (2018) Phosphorus-doped graphene-based electrochemical sensor for sensitive detection of acetaminophen. Anal Chim Acta 1036:26–32
32. Zhou X, Ye Z, Zheng X, Hong Z (2017) Fabrication of carbon@co nanocages/nafion/poly tiopronin composite film and its application for determination of acetaminophen. J Electrochem Soc 164:B513–B518
33. Li F, Li R, Feng Y, Gong T, Zhang M, Wang L, Meng T, Jia H, Wang H, Zhang Y (2019) Facile synthesis of au-embedded porous carbon from metal-organic frameworks and for sensitive detection of acetaminophen in pharmaceutical products. Mater Sci Eng C 95:78–85